Corrosion Science xxx (xxxx) xxx–xxx

Contents lists available at ScienceDirect

Corrosion Science

journal homepage: www.elsevier.com/locate/corsci

Comparison of the oxidation behavior of a zirconium nitride coating in water vapor and air at high temperature

Zhaohe Gao[a], Ying Chen[a], Justyna Kulczyk-Malecka[a,b], Peter Kelly[b], Yi Zeng[a], Xinxin Zhang[a], Chun Li[a], Han Liu[a], Nadia Rohbeck[a], Ping Xiao[a,*]

[a] School of Materials, University of Manchester, Manchester, M13 9PL, UK
[b] Surface Engineering Group, Manchester Metropolitan University, Manchester, M1 5GD, UK

ARTICLE INFO

Keywords:
Zirconium nitride
Water vapor
Oxide cracks
Phase transition
Oxidation kinetic
Oxidation mechanism

ABSTRACT

The oxidation behavior of zirconium nitride coating in high-temperature water vapor and air environments was studied. The parabolic rate constant of ZrN oxidizing in the water vapor environment at 600 °C was approximately 100 times faster than that in air, due to the larger pores and greater number of cracks that were formed across ZrO_2 oxide layer formed during the water vapor oxidation process than during the air oxidation process. A bilayer-structure ZrO_2 with tetragonal ZrO_2 near the ZrN/ZrO_2 interface and monoclinic ZrO_2 approaching the outer ZrO_2 surface were formed in both cases. The lateral cracks across the ZrO_2 scale were caused by volume expansion from the tetragonal ZrO_2 phase to the monoclinic ZrO_2 phase transition.

1. Introduction

Since the nuclear disaster occurred at the Fukushima Daiichi Power Plant on March 2011 owing to a Loss-of-Coolant Accident (LOCA) in the Light Water Reactor, concerns over the safety of nuclear power plants in the case of a cooling system failure have been raised. When a LOCA occurs, the zirconium fuel cladding quickly reacts with the high-temperature water vapor generated by the fission product decay heat trapped inside the nuclear reactors [1,2]. The reaction produces a large amount of hydrogen in a short period of time, which is highly flammable and upon ignition can lead to an explosion.

One potential strategy to mitigate LOCA from occurring is to apply an oxidation-resistant coating onto the surface of the zirconium fuel cladding. To date, a few metallic (*e.g.* FeCrAlY) and ceramic (*e.g.* Ti_2SiC, TiN) coatings have been deposited on zirconium alloys and been tested in different environments [3,4]. These coatings have been shown to slow down the oxidation rate of the zirconium alloys in air or water vapor to a certain extent. However, none of these coatings have shown satisfactory durability which is required in case of failure of the cooling system in nuclear power plants.

From the perspective of practical application, an effective coating on the zirconium fuel cladding should be protective, thermally stable, thermally conductive, well-adhered to the metal substrate, mechanically robust and have a low neutron capture cross-section. A potential candidate material that meets these criteria, apart from the coating materials reported in the literature, is zirconium nitride (ZrN). The main reasons that ZrN coating is good candidate are its high oxidation resistance, high thermal conductivity and low neutron capture cross-section [5–7]. The majority of current studies of ZrN have focused on its oxidation behavior and products in air, which is significantly different from the high temperature water vapor environment encountered by the zirconium fuel cladding in case of cooling system failure [8,9].

Harrison, Lee, and Jacobson studied the oxidation of ZrN from 973 to 1373 K under static air conditions and reported a parabolic rate behavior indicative of a diffusion-controlled process [8]. Others have confirmed that the oxidation kinetics of ZrN in the high temperature air follows a parabolic relation while there are disagreements related to the phase structure (tetragonal or monoclinic) of the ZrO_2 formed on the ZrN [10]. To the best of our knowledge, we are not aware of any study of the oxidation behavior and oxidation kinetics of ZrN in a water vapor environment at high temperature. It is expected that metals and ceramics show different oxidation behavior and oxidation mechanism in air and steam at high temperature. For example, Kyung Tae Kim, et al, found that the high-temperature (700 °C to 1200 °C) oxidation kinetics of Zr alloy in the air were more rapid than that in the steam [11]. Dong Jun Park, et al, reported that the SiC showed two different oxidation behaviors in the air and water vapor environment at 1200 °C and SiC underwent weight gain and weight loss during oxidation in air and steam, respectively [12].

To address this research gap and to understand the oxidation behavior of ZrN in water vapor and test if ZrN might be used as an effective coating material in zirconium fuel cladding, the oxidation

* Corresponding author.
E-mail address: p.xiao@manchester.ac.uk (P. Xiao).

https://doi.org/10.1016/j.corsci.2018.04.015
Received 21 May 2017; Received in revised form 3 April 2018; Accepted 9 April 2018

behavior of a ZrN coating deposited on a zirconium alloy substrate in high temperature water vapor was systematically studied in this work. The ZrN coating was deposited using reactive magnetron sputtering, a technique, which offers excellent uniformity of the coating layer. The oxidation behavior of the ZrN coating in air was also studied in order to compare the difference of the oxidation behavior and oxidation kinetics of the coating in these two environments.

Finally, observation of the ZrO_2 scales formed on the ZrN after oxidation in an air environment has revealed the existence of cracks and pores [9]. The phase structure of the ZrO_2 and the cracks themselves are generally believed to play an import role in the oxidation process of ZrN during high-temperature air [8]. However, it is not fully understood how the cracks are generated and the effects of oxide scale on the oxidation mechanism of ZrN in the air. And the morphology of the oxide scale formed on ZrN in the water vapor environment at high temperature and the related oxidation mechanism are also unknown. Thus, the formation mechanism of cracks and pores and the effect of the oxide scales on the oxidation mechanism of ZrN in the high temperature air and water vapor have also been studied.

2. Experiments

2.1. Sample preparation and oxidation test

The ZrN coatings were deposited on Zr2.5 wt%Nb alloy coupons ($100 \times 50 \times 2\,mm^3$), which were ultrasonically pre-cleaned in acetone. Deposition took place by reactive sputtering in a Teer Coatings UDP 350 closed field unbalanced magnetron sputtering system, described in detail elsewhere [13]. Two vertically mounted magnetrons ($300 \times 100\,mm^2$) were installed in opposed positions through the chamber walls in a closed field configuration, with a centrally mounted rotating substrate holder. A 99.5% pure Zr target was fitted to one of the magnetrons and the second magnetron was blanked off; it was present only to close the magnetic field lines across the chamber. Prior to deposition, the chamber was pumped down to a base pressure of lower than 1×10^{-3} Pa and then backfilled to a working pressure of 0.3 Pa with argon. The substrates were sputter cleaned at a bias voltage of −800 V DC for 10 min. The zirconium target was powered by a dual channel Advanced Energy Pinnacle Plus power

supply operating in pulsed DC mode at an average power of 1 KW and a pulse frequency of 100 kHz with a 4.0 μs off time (duty cycle = 60%). To ensure good coating to substrate adhesion, an initial 50 nm interlayer of pure zirconium was deposited in an argon only atmosphere. The optical emission monitoring (OEM) system was used to control the amount of nitrogen introduced into the system during the deposition of ZrN films, using settings based on previous experience to produce a stoichiometric coating [13,14]. The Ar flow rate was 20 standard cubic centimetres per minute (SCCM) and N_2 was controlled using optical emission monitor (OEM) set at 50% total metal (Zr) signal. A bias of −50 V was applied to the substrate throughout coating deposition. The substrate temperature under the sputtering conditions was below 200 °C. Rectangular samples (10 × 10 mm) were cut from the ZrN-coated alloy plates using a SiC abrasive cutting blade in a precision cut-off machine (Accutom 5, Struers). The samples were then cleaned with soap water and acetone.

Oxidation in water vapor was conducted by flowing a mixture of argon and water vapor through a universal tube furnace (Carbolite, UK) at 600 °C for different periods of time up to 2 h. The flowing argon first flowed through a flask containing ~400 ml boiling water which generated sufficient amount of water vapor. The water vapor

was then carried by the flowing argon to the hot zone of the furnace where the samples were placed.

In order to control the volume content of the water vapor during oxidation, the mass of the flask before and after the experiment was measured. The volume of the water vapor flowing over the surface of the sample was 1.74 L/min. Oxidation in air was conducted by placing the samples in the centre of the hot zone of the same furnace and heating it up to 600 °C in the ambient flowing air. In order to minimise the oxidation during ramping and down, the samples were directly put inside the furnace when the temperature stabilised at 600 °C and then taken out after oxidation.

2.2. Microstructural characterization and stress measurement

The phase composition of the ZrN coating and oxides was analysed by grazing incidence X-ray diffraction (GIXRD, Philips X,pert) using Cu Kα radiation (λ = 1.5406 Å). The surface and cross-section of the ZrN coatings and oxides were investigated by scanning electron microscopy (SEM, FEI, Quanta 650) coupled with a focused ion beam (FIB, FEI, Quanta 3D). The thickness of the oxides was estimated from the cross-section exposed by FIB milling through the surface. Tilt correction was implemented to compensate for the distortion of the image induced by tilting. To observe the microstructure of the oxides in greater detail, thin lamellas of the cross-sections of the oxides were prepared by FIB using the *in situ* lift-out technique and then examined using transmission electron microscopy (TEM, FEI, Tecnai G2).The phase distribution in the oxides was mapped using a transmission electron backscatter diffraction performed on an FEI Magellan 400 XHR scanning electron microscope (SEM). This technique is known for its high resolution, which has been shown to be particularly useful in analysing materials with fine grains. More details of this technique can be found elsewhere [15]. The Gibbs reaction energy between ZrN and oxygen and ZrN and water vapor, was calculated using Thermocalc 4.0 software and the calculation followed the Calphad rules.

The biaxial stress in the ZrO_2 oxide layer was measured by XRD using the $\sin^2\psi$ method carried out in a Bruker D8 Discover x-ray diffractometer. An X-ray tube (Co, λ = 1.789 Å) was fixed with an incident beam angel of 5° during the measurement. The detector enables the ψ (the angle between the surface normal and the bisector of the incident and diffracted beam) offset to be measured simultaneously. Co Kα radiation (λ_{Co} = 1.78897 Å) was used to acquire the diffraction peak from the (−1 1 1) plane of monoclinic ZrO_2 for all the measurements. The geometry configuration is shown in Fig. 1. The XRD measurements give a series of d-spacing values corresponding to different ψ angles. These d-spacing values were then plotted against $\sin^2\psi$, which were then fitted with a straight line. The slope of the line was used to calculate the residual stress (σ) according to the formula [16,17]:

$$\sigma = \left(\frac{E}{1+\nu}\right)_{(hkl)} \frac{1}{d_n} \frac{(d_\omega - d_n)}{sin^2\omega}$$

where E and ν are the elastic modulus (243 GPa) and Possion,s ratio (0.28) of the (−1 1 1) plane, respectively [18]. And value of d_n was the d-spacing along the surface normal (when ψ = 0). The d_n was estimated based on the (−1 1 1) diffraction peak using Cu Kα radiation (λcu = 1.5406 Å) under the Θ/2Θscanning configuration in a powder X-ray diffractometer (Philips PANalytical X,Pert).

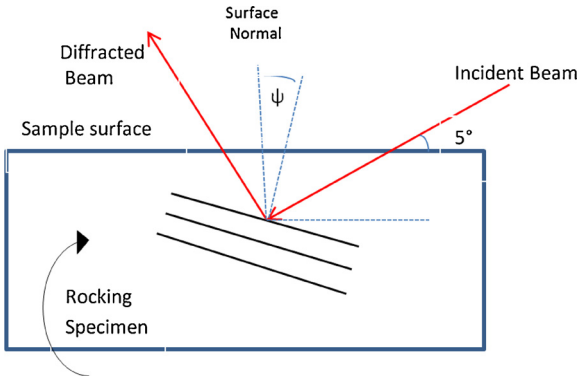

Fig. 1. Geometry of stress measurement by Bruker Discover XRD.